Helmholtz-Zentrum Geesthacht
Zentrum für Material- und Küstenforschung

Final Draft
of the original manuscript:

Eggers, S.; Lauterbach, F.; Abetz, V.:

Synthesis and self-assembly of high molecular weight polystyrene-block-poly[2-(N-morpholino)ethyl methacrylate]: A story about microphase separation, amphiphilicity, and stimuli-responsivity

In: Polymer (2016) Elsevier

DOI: 10.1016/j.polymer.2016.04.066

Full Paper

Synthesis and Self-assembly of High Molecular Weight Polystyrene-*block*-poly[2-(*N*-morpholino)ethyl methacrylate]: A Story about Microphase Separation, Amphiphilicity, and Stimuli-responsivity

Steffen Eggers [a], Felix Lauterbach [a], Volker Abetz [a,b,*]

[a]University of Hamburg, Institute of Physical Chemistry, Martin-Luther-King-Platz 6, 20146 Hamburg, Germany

[b]Helmholtz-Zentrum Geesthacht, Institute of Polymer Research, Max-Planck-Straße 1, 21502 Geesthacht, Germany

* Corresponding author. E-Mail address: volker.abetz@hzg.de.

The synthesis of polystyrene-*block*-poly[2-(*N*-morpholino)ethyl methacrylate] (PS-*b*-PMEMA) as a new highly amphiphilic and multiple stimuli-responsive block copolymer is presented. To achieve high molecular weights far beyond 100 kDa in a highly controlled manner (dispersities < 1.1), a synthetic route *via* sequential combination of anionic polymerization for the PS block and reversible addition–fragmentation chain transfer (RAFT) polymerization for the PMEMA block is used. The synthesized block copolymers are investigated regarding their microphase separation in bulk, which delivers well-ordered self-assembled bulk structures as evidenced by small-angle x-ray scattering (SAXS) and atomic force microscopy (AFM). In aqueous solution, the block copolymer self-assembles into narrowly size distributed micelles with a PMEMA corona. The stimuli-triggered micelle response towards temperature, pH, and kosmotropic as well as chaotropic salts is shown *via* various dynamic light scattering (DLS) experiments. Furthermore, a dependency of aggregate size on solvent composition in polymer/tetrahydrofuran/water mixtures is described. The reported findings deliver a feasible pathway to high molecular weight block copolymers with tailored chemical properties and show the potential of PS-*b*-PMEMA as material for mechanically demanding switchable devices.

1. Introduction

In the last two decades, enormous progress was made in developing feasible controlled polymerization methods. Especially the discovery and optimization of controlled radical polymerizations (CRPs),[1] such as nitroxide-mediated radical polymerization (NMP),[2] atom transfer radical polymerization (ATRP)[3,4] and reversible addition–fragmentation chain transfer (RAFT) polymerization,[5] made the viability of controlled polymerizations relatively straight forward. Thus, polymers with tailored complex structures, *e.g.* block copolymers (BCPs), gradient copolymers, telechelics or polymer brushes, can nowadays be accessed by a broad scientific community beyond specialized polymer chemists. Indeed, this leads to application-tailored polymers being used in various fields of biology, drug delivery, surface modification and patterning, lithography and membrane science, just to mention a few.[6-11] Particularly BCPs have found a way into many fields of research and concrete potential applications. Those polymers self-assemble into distinct bulk structures, spheres, cylinders, gyroids or lamellae, if the product of interaction parameter χ and total degree of polymerization N is sufficiently high.[12] In a selective solvent for one of the blocks, the BCPs form aggregated structures, *i.e.* spherical micelles, cylindrical/worm-like micelles or vesicles/polymersomes, depending on the block volume fractions and lengths.[13-15]

The discovery and development of stimuli-responsive polymers significantly increased opportunities and applications of BCP micelles. The term 'stimuli-responsivity' means that the dissolved polymer instantaneously and reversibly changes its solubility upon change of certain conditions, most often temperature, pH, salt-concentration or light. On a molecular level, the responsivity of aqueous polymer solutions is referred to the existence of H-bonds in between polymer and water. The distinct orientation of such H-bonds results in a negative orientational entropy, which is why they break at higher temperatures for thermodynamic reasons.[16] This induces a coil-to-globule transition of the polymer chain followed by aggregation and precipitation.[17] If introduced into BCP micelles, that leads to stimuli-triggered micellization (if one block is stimuli-responsive) or schizophrenic micelles (if two blocks oppositionally respond to a stimulus).[18-20]

Poly[2-(*N*-morpholino)ethyl methacrylate] (PMEMA) (Figure 1) is known to be a multiple stimuli-responsive polymer as it shows a lower critical solution temperature (LCST) at 32–53 °C, depending on molecular weight (MW), pH-responsivity due to the basic morpholino groups in its side chains (pK_a of the conjugated acid ≈ 4.9) and a pronounced salt-responsivity.[21-23] Furthermore, biocompatible PMEMA as a part of copolymers was recently tested regarding the delivery of drugs in cancer treatment applications, indicating the high potential of stimuli-responsive polymers in general and of PMEMA in specific in nanomedical applications.[24,25] Also, our group recently published a systematic study about the peculiar multi-step aggregation behavior of PMEMA upon heating, which brought up interesting insights into macromolecular aggregation processes from a mechanistic point of view.[21]

Of the different controlled polymerization methods, living anionic polymerization appears to be the one delivering the best control. This goes back to the fact that statistical irreversible termination and transfer processes are almost fully suppressed and initiation is much faster than propagation.[26] Also, high MWs above 100 kDa are easily achievable as a result of the rather fast chain growth compared to other methods. Nevertheless, application of anionic polymerization is limited to electron deficient non-acidic monomers with no functional groups being prone to nucleophilic attack of the growing reactive anion. In addition, it is experimentally demanding because of its high sensitivity towards impurities, such as oxygen or water. On the other hand, CRPs such as RAFT polymerization are versatile to polymerize a huge number of monomers containing vinylic double bonds due to the high tolerance towards functional groups.[27] At the same time, RAFT polymerization is experimentally easy to

conduct and rather robust concerning slight impurities. In fact, RAFT polymerizations in an open vessel were published in the last two years, utilizing oxygen consuming additives like glucose oxidase,[28] organo-dyes[29] or strongly reductive transition metal catalysts.[30,31] As was reviewed recently by Hill *et al.*, though, the RAFT technique still has certain challenges, *e.g.* the unavailability of high MW polymers from low k_p monomers.[32] For instance, styrenes and methacrylates as highly significant monomers belong to this class.
Regarding the formerly mentioned pros and cons of both methods, high MW amphiphilic BCPs made from a major hydrophobic block and a minor hydrophilic chemically more sophisticated block can best be synthesized *via* combination of both anionic and RAFT polymerization. Such combination is described in a handful of publications in the recent years. It is mostly performed by hydroxyl functionalization of the anionically synthesized block, followed by esterification with a carboxyl functionalized RAFT agent.[33-35] However, Zhang *et al.* published a way to in situ switch from anionic to RAFT polymerization *via* end capping of the active polymeric anion with diphenylethylene (DPE) and subsequent nucleophilic attacks on CS_2 and alkyl halide.[36] While in mechanically demanding applications (*e.g.* in ultrafiltration devices) high MW BCPs are needed due to their higher mechanical toughness caused by chain entanglements, most publications present the synthesis of low MW BCPs *via* the discussed combination pathway. This, most likely, goes back to the fact that determination of end functionalization degree of the first block is limited to short polymer chains. Actually, Pafiti *et al.* published one of the rare examples in which it was dealed with MWs above 100 kDa for the synthesis of polystyrene-*block*-poly[vinylpyridines] (PS-*b*-P4VP/P2VP).[35]
By far the most common method for hydroxyl end capping of the growing polymeric anion is the chain growth termination with ethylene oxide (EO). The created alkoxy anion with EO addition does not attach further epoxide molecules as a result of its high stabilization by the Li^+ counter ion (originating from alkyl lithium initiator) and, hence, quenches polymerization.[37] Quirk *et al.* published a series of works on end capping with other epoxides, *e.g.* styrene oxide (SO)[38,39] and propylene oxide (PO).[40] Although PO as most of the short chain epoxides is toxic, it is liquid at room temperature and, thus, easier and safer to handle than gaseous EO. At the same time, the boiling point (bp) of PO is relatively low (34 °C under atmospheric pressure), making its purification *via* distillation fairly easy (as opposed to *e.g.* SO, bp = 194 °C).

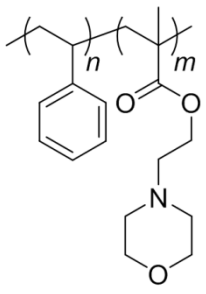

$\overline{M}_n \leq 240$ kDa, $Đ < 1.1$

Figure 1 Simplified chemical structure of the investigated block copolymer polystyrene-*block*-poly[2-(*N*-morpholino)ethyl methacrylate].

In this work, we present a feasible synthetic route to well-defined high MW (up to $\overline{M}_n \approx 200$ kDa) PS-*b*-PMEMA BCPs (Figure 1) *via* sequential combination of anionic (for the PS block) and RAFT polymerization (for the PMEMA block). The presented method is supposed to be the most versatile (if not the only) one to obtain high MW BCPs with a highly functionalized minor block, while achieving very low MW dispersities ($Đ < 1.1$). To the best of our knowledge, this is the first time synthesis as well as remarkable properties of PS-*b*-

PMEMA as a multiple stimuli-responsive BCP are published. Syntheses of other amphiphilic BCPs with comparable high MWs can hardly be found *via* the presented synthetic route. Additionally, the distinct self-assembly of the synthesized BCPs is extensively investigated in bulk and in aqueous solution, showing interesting stimuli-triggered micelle features. The latter is especially relevant when a potential application of the BCPs in self-assembling switchable devices is envisaged.

2. Experimental

2.1. Materials

All chemicals were purchased with the highest purity as possible and were used without further purification unless otherwise noted. Azobisisobutyronitrile (AIBN) was recrystallized twice from methanol and stored at −20 °C. Monomers styrene and MEMA were passed through a short column of basic alumina (Brockmann I) prior to use to remove the inhibitor mono methyl ether hydroquinone (MEHQ). Ultrapure water (type I, 18.2 MΩ cm^{-1}) was obtained from a Millipore water purification system. For anionic polymerization, THF as solvent was stored over molecular sieve (4 Å), freshly distilled prior to use and degassed by a freeze–pump–thaw cycle. ^{s}BuLi was added slowly at −30 °C until the resulting yellow color lasted for at least 20 min, indicating sufficient purity of the THF. Inhibitor-free styrene was stored over $^{n}Bu_2Mg$, freshly distilled into ampulla prior to use and degassed by two freeze–pump–thaw cycles. Propylene oxide (PO) was stirred for 1 h over CaH_2 at 0 °C, distilled into ampulla and degassed by a freeze–pump–thaw cycle prior to use. All described distillation steps were conducted in static vacuum.

2.1.1. Anionic Polymerization of Styrene

A typical anionic polymerization of styrene was conducted as follows:
THF (200 mL) was frozen, degassed and styrene (17.0 mL, 149 mmol, 1183 eq) was added from ampulla into the frozen flask *via* distillation. The mixture was allowed to warm up to −70 °C and ^{s}BuLi (1.4 M in cyclohexane) (0.09 mL, 126 µmol, 1.0 eq) was added rapidly under an argon atmosphere and vigorous stirring by means of a syringe. Stirring of the yellowish solution was continued at −70 °C for 1 h and PO (0.20 mL, 2.9 mmol, 23 eq) was added rapidly to the polymerization solution *via* syringe to terminate the polymerization. The colorless solution was allowed to warm up to −30 °C for 3 h. A solution of acetic acid in MeOH (5:95, *v/v*) (5.0 mL, 4.4 mmol, 35 eq) was added *via* syringe and the solution was allowed to warm up to room temperature for 30 min. The resulting hydroxyl functionalized PS (PS–OH) was precipitated twice from cold methanol (2.0 L). Drying *in vacuo* at room temperature for 2 days delivered the polymer as a colorless solid.

SEC: $\overline{M}_n$ = 111 kDa, $Đ$ = 1.02; ^{1}H NMR spectroscopy (400 MHz, $CDCl_3$): δ (ppm) = 7.31–6.87 (m, 3H, aromatic H_{ortho}, H_{para}), 6.87–6.29 (m, 2H, aromatic H_{meta}), 3.58–3.21 (m, end group –C*H*(CH_3)OH), 2.31–1.15 (m, 3H, backbone *H*).

2.1.2. Steglich Esterification of Hydroxyl Functionalized Polystyrene

A typical conversion of PS hydroxyl end function to the dithioester end function suitable for a RAFT polymerization followed in principle a published procedure by Pafiti *et al.*[35] Equivalents of RAFT agent 4-cyano-4-(phenylcarbonothioylthio)pentanoic acid (CPADB) and *N,N'*-dicyclohexylcarbodiimide (DCC) relative to PS–OH as well as reaction times were varied with polymer chain length (see below).
PS–OH (5.0 g, 44.0 µmol, 1.0 eq), CPADB (630 mg, 2.30 mmol, 52 eq) and 4-dimethylaminopyridine (DMAP) (2.7 mg, 22.0 µmol, 0.5 eq) were dissolved in anhydrous dichloromethane (DCM) (18.0 mL) and DCC (500 mg, 2.40 µmol, 55 eq) in DCM (1.6 mL) was added dropwise at room temperature. The purple turbid solution was stirred overnight. The precipitated urea side product was removed *via* filtration, the clear solution was diluted with DCM to approximately twice its initial volume and the polymer was precipitated four times in cold MeOH (1.0 L) until washings were colorless, indicating absence of unconverted CPADB. The polymer was dried *in vacuo* at room temperature for 2 days to obtain the PS macroRAFT agent as a pale purple solid.

SEC: $\overline{M}_n$ = 111 kDa, $Đ$ = 1.02; ^{1}H NMR spectroscopy (400 MHz, $CDCl_3$): δ (ppm) = 7.31–6.87 (m, 3H, aromatic H_{ortho}, H_{para}), 6.87–6.29 (m, 2H, aromatic H_{meta}), 4.80–4.40 (m, end group –C*H*(CH_3)OC(O)–), 2.31–1.15 (m, 3H, backbone *H*).

Chain length specific reaction conditions were chosen as follows:
$\overline{M}_n$ = 6 kDa: equivalents CPADB and DCC = 5, reaction time = 2 h. $\overline{M}_n$ = 56 kDa: equivalents CPADB and DCC = 25, reaction time = overnight. $\overline{M}_n$ = 90–130 kDa: equivalents CPADB and DCC = 52, reaction time = overnight. $\overline{M}_n$ = 171 kDa: equivalents CPADB and DCC = 75, reaction time = 24 h.

2.1.3. Chain Extension of Polystyrene macroRAFT Agent with MEMA *via* RAFT Polymerization

The polymerizations were conducted in a thermomixer including a heated aluminum block and a shaking device, utilizing 10 mL glass vials with bored screw caps equipped with silicone/polytetrafluoroethylene (PTFE) seals. A typical RAFT polymerization of MEMA using PS macroRAFT as RAFT agent was conducted as follows:
MEMA (1.22 g, 6.10 mmol, 1119 eq) and the PS macroRAFT agent (600 mg, 5.5 µmol, 1.0 eq) were dissolved in 1,4-dioxane/toluene (3:1, *v/v*) (7.2 mL) and AIBN (0.09 mg, 0.55 µmol, 0.1 eq) in 1,4-dioxane/toluene (3:1, *v/v*) (60 µL) was added. The solution was deoxygenated *via* N_2 bubbling for 15 min at 0 °C and subsequently shaken at 65 °C in the absence of oxygen. The polymerization was quenched by cooling down the solution to 0 °C and exposure to air. The solution was diluted with THF to approximately double of its initial volume and the polymer was precipitated twice by dropwise addition to rapidly stirring cold ^{n}hexane (100 mL). The pale purple BCP was dried *in vacuo* at room temperature for 2 days.

^{1}H NMR spectroscopy (400 MHz, $CDCl_3$): δ (ppm) = 7.31–6.87 (m, 3H, PS aromatic H_{ortho}, H_{para}), 6.87–6.29 (m, 2H, PS aromatic H_{meta}), 4.05 (m, 2H, PMEMA –C(O)OC$H_2$$CH_2$–), 3.68 (m, 4H, PMEMA morpholine O(C$H_2$$CH_2$–)$_2$), 2.59 (m, 2H, PMEMA –NC$H_2$$CH_2$–), 2.48 (m, 4H, PMEMA morpholine –N(C$H_2$$CH_2$–)$_2$), 2.31–0.67 (m, 8H, backbone *H*, PMEMA CH_3). See also Figure S2. More sample specific analytical data are presented in Table S2.

2.2. Analytics

Size-exclusion chromatography (SEC) was conducted on a system PSS Agilent Technologies 1260 Infinity consisting of a precolumn (8 mm × 50 mm) and three analytical columns (8 mm × 300 mm) with cross-linked styrene divinylbenzene (SDV) as stationary phase, SECcurity auto injector and an isocratic SECcurity pump. The system was operating with the software WinGPC, a refractive index and a UV-Vis detector, working at a wave length of 260 nm. As eluent, tetrahydrofuran (THF) with a flow rate of 1.0 mL min^{-1} at a temperature of 30 °C was utilized, toluene was added as an internal standard. The injection volume was 100 µL. The analyzed polymer solutions had concentrations of 1 g L^{-1}. For determination of relative MWs and *Đ*-values, the system was calibrated with narrowly distributed PS standards.

^{1}H NMR spectroscopy was used for determination of monomer conversion in the RAFT step (Figure S1), weight fractions and MWs of the BCPs (Figure S2) as well as end group functionalization degree (Figure 2). The NMR experiments were conducted on a Bruker AvanceII 400 MHz spectrometer. For a typical ^{1}H NMR spectrum, 16 scans were recorded and a relaxation delay of 3 s was applied. Solutions were measured in $CDCl_3$ at concentrations of approximately 20 g L^{-1}. For end group estimation, signal-to-noise ratio was increased by recording 1024 scans per spectrum while using concentrations of 50 g L^{-1}. The residual solvent signal at 7.26 ppm was used as internal reference for the chemical shifts. The spectra were analyzed with the software MestReNova 7.1.

2.2.1. Film Preparation, Atomic Force Microscopy (AFM) and Small-angle X-ray Scattering (SAXS)

BCP thick films (thickness ≈ 1 mm) were made *via* slow evaporation (roughly 7 days) of the solvent from a BCP solution in THF ([BCP] = 5 wt%). The glass vials filled with polymer solution were shaken for 24 h to guarantee full dissolution and were subsequently placed in a desiccator with THF atmosphere from which the solvent was allowed to slowly evaporate in a controlled manner. After complete drying, films were obtained by cooling the vials with liquid N_2 and cautiously cracking the glass.

AFM images of the BCP microphase separation in bulk were recorded with a JPK NanoWizard Instrument in intermittent contact mode under atmospheric conditions using the NanoWizard Control software. A silicon tip with a radius of 10 nm, a resonant frequency of 300 kHz and a force constant of 40 N m^{-1} was used. The software Gwyddion (Version 2.31) was used to process the raw data.

SAXS images were recorded at EMBL/DESY Petra III synchrotron, beamline P12, in Hamburg (Germany). An energy of 10 keV (λ = 1.24 Å), a beam size of 0.1 mm × 0.2 mm (width × height) and a Pilatus 2M detector at a sample-to-detector distance of ca. 3.0 m were used. The total exposure period was 1 s, while 20 frames were taken for each sample. An empty sample holder was measured to subtract background.

2.2.2. Micelle Preparation and Dynamic Light Scattering (DLS)

All solvents were passed through filters (hydrophilic cellulose or hydrophobic PTFE) with average pore diameters of 200 nm prior to use to remove any macroscopic dust particles. For micelle preparation, the BCP was dissolved in THF overnight ([BCP] = 1.0 wt%) and the solution was added dropwise through a hydrophobic PTFE filter (average pore diameter = 200 nm) to stirred water such that the final BCP concentration was 0.01 wt% (water/THF ≈ 100:1 (*w/w*)). The system was equilibrated for 1 day under slight stirring, while

the residual THF was allowed to evaporate. Variation of pH-value (apparent pH, calculated from HCl concentration in solution volume) was achieved by HCl addition to an aqueous micellar solution and equilibrating overnight. Different salt concentrations were adjusted by addition of 5 M aqueous solutions of the respective sodium salt to an aqueous micellar solution and equilibrating overnight. For generating different ratios of organic solvent (THF or 1,4-dioxane) and water, a specific amount of water was added to a stirred solution of the BCP in the respective organic solvent ([BCP] = 0.05 wt%) and the system was equilibrated overnight under slight stirring.

DLS measurements were conducted on an ALV/CSG-3 Compact Goniometer-System using a ALV/LSE-5003 Multiple Tau Digital Correlator working with pseudo cross correlation and the ALV Digital Correlator Software 3.0. The measuring angle was set to 90° for all measurements, every single measurement was conducted for 30 s. As light source, a Nd:YAG laser emitting at 532 nm was used. The sample vials consisted of quartz glass and were placed into a measurement cell filled with toluene. The toluene bath was tempered by a Julabo F25 thermostat working with a mixture of water and ethylene glycol and delivering a temperature accuracy of 0.01 °C.

Results for room temperature measurements of the micelles are arithmetic averages of at least 10 measurements. Temperature-dependent measurements were conducted in temperature steps of 0.5 °C with one measurement per temperature. Each temperature was stabilized for 3 min prior to measurement.

The viscosity and refractive index of the solution were automatically corrected with temperature according to tabulated values of the solvent, *i.e.* water, THF/water mixtures or 1,4-dioxane/water mixtures.[41] Diffusion coefficient (*D*) was calculated automatically by the DLS software from the averaged relaxation rate $\bar{\Gamma}$ by fitting the field autocorrelation function $g^1(q,t)$ with a cumulant up to second order:

$$\ln\left(g^1(q,t)\right) = \ln A \; - \; \bar{\Gamma} \times t + \frac{\mu_2}{2} \times t^2. \qquad (1)$$

q: wave vector. *t*: time. *A*: amplitude. The size dispersity $\frac{\mu_2}{\bar{\Gamma}^2}$ of the particles was calculated from the second moment μ_2.

Hydrodynamic radius (R_h) was estimated from *D via* the Stokes–Einstein equation.

3. Results and Discussion

3.1. Synthesis of PS–OH and PS macroRAFT

In this work, a synthetic pathway to highly amphiphilic stimuli-responsive BCPs of MWs as high as 200 kDa is described. To synthesize the major hydrophobic PS block, anionic polymerization was utilized while the minor stimuli-responsive PMEMA block was subsequently synthesized *via* RAFT polymerization. To create a suitable macroRAFT agent from the PS block, a route *via* end functionalization with hydroxyl function and ensuing Steglich esterification with a carboxyl functionalized RAFT agent was used (Figure 2). Analytical data of the obtained polymer samples (PS macroRAFT agents) are included in Table S1. After complete monomer consumption in the anionic polymerization step, an excess of PO is added to generate an alkoxy anion *via* nucleophilic attack of the carbanion at the lower substituted carbon of the PO.[38,40] Subsequently, protonation with acetic acid delivers a hydroxyl end group which can further be converted into a dithiobenzoate end group *via* Steglich esterification. In this step, a higher excess of carboxyl functionalized RAFT agent CPADB and DCC (for acid activation) is necessary with higher PS–OH chain length. This is caused in higher steric shielding of the end function and therefore in a kinetic inhibition of the

esterification.[35] An increased amount of catalyst DMAP above 0.5 eq, however, lead to significant loss of RAFT end group functionality, being most likely due to nucleophilic side reactions of DMAP with the formed ester.
The successful conversion of the hydroxyl group into the ester can be monitored by a downfield shift of the related α-proton, if the MW of the PS–OH is not too high (Figure 2). Remarkably, this proton gives two broad peaks at 3.3 and 3.5 ppm with intensity ratio 1:1 in the case of the alcohol and three peaks at 4.7, 4.6 and 4.5 ppm with intensity ratios 1:1:2 for the ester. Most likely, this goes back to the formation of diastereomers as indicated in Figure 2, though the effect on the magnetic environment of the α-proton is surprisingly strong and ranges over multiple bonds.

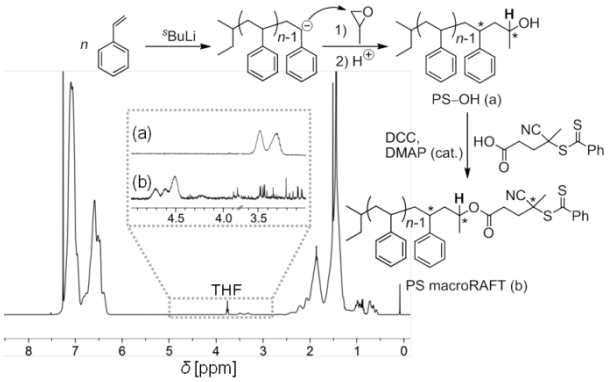

Figure 2 Synthetic pathway to a polystyrene macroRAFT agent (PS macroRAFT (b)) *via* anionic polymerization of styrene, end functionalization with hydroxyl group (PS–OH (a)) and Steglich esterification. The ^{1}H NMR inset (residual THF peak at 3.76 ppm removed for clarity) shows the downfield shift of the α-proton (marked in bold) upon esterification. Stereocenters are marked with "*".

As a result, it can be concluded that synthesis of narrowly distributed PS macroRAFT agents with MWs from 5 kDa to 170 kDa and very low *Đ*-values down to 1.02 was successful. Nevertheless, especially in case of high MW PS–OH, the functionalization degree can hardly be determined *via* ^{1}H NMR spectroscopy because the end group concentration becomes very low. In those cases, a quantitative chain extension in the RAFT polymerization step is the only indicator for a successful end functionalization.

3.2. Chain Extension of PS macroRAFT with MEMA *via* RAFT Polymerization

The synthesized PS macroRAFT agents were used to polymerize MEMA *via* a RAFT process, attaching a multiple stimuli-responsive block to the highly hydrophobic PS block. Exemplary analytical data for a series of synthesized BCPs are given in Table S2. The inherent challenge in the presented synthesis is the highly different polarity of the two blocks, making the choice of polymerization medium crucial. Furthermore, extending a high MW PS macroRAFT agent suffers from high kinetic inhibition of the radical chain growth (chain length dependent k_p) by steric shielding and, thus, a reduced local monomer concentration around the active chain end.[42] Therefore, polymerization conditions such as solvent, choice of initiator and [RAFT]/[initiator] had to be carefully optimized, which was indeed extensively performed exemplary for PS macroRAFT^{111}.

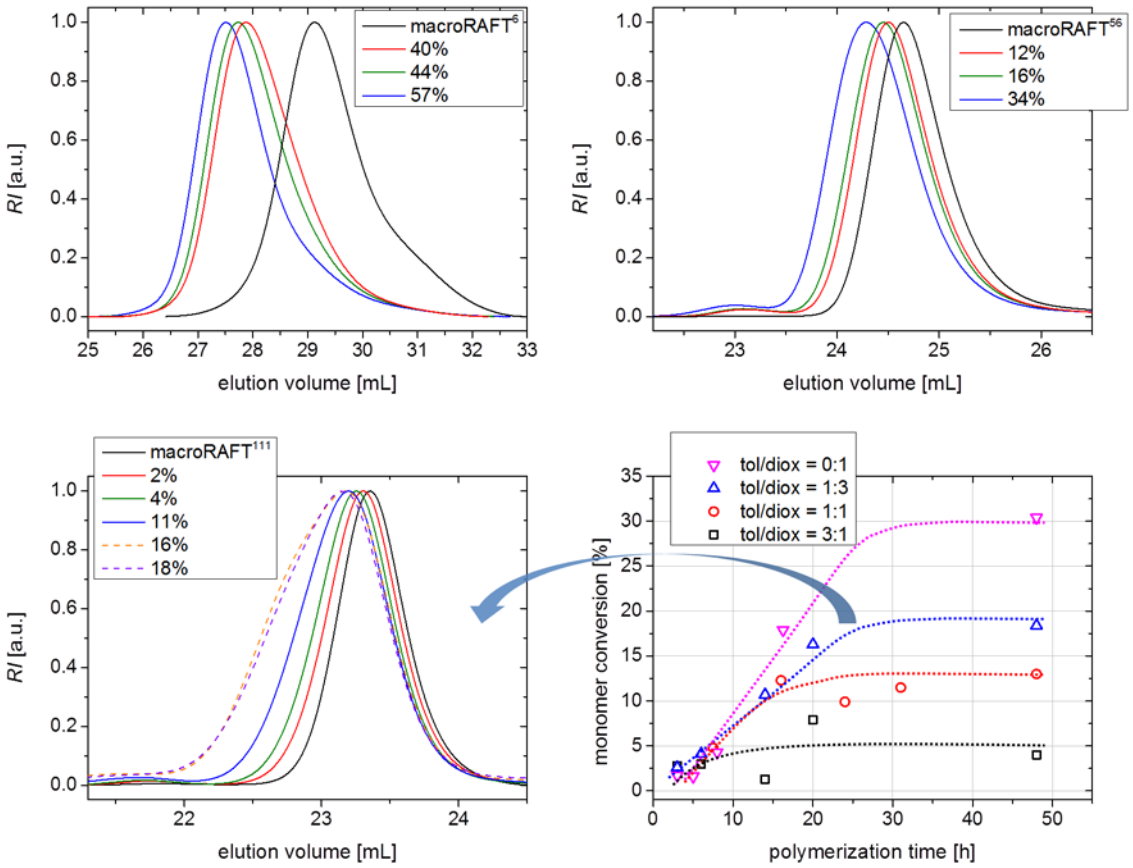

Figure 3 SEC traces (relative signal intensity (*RI*) *versus* elution volume) of various block copolymers gained by chain extension of polystyrene macroRAFT agents with MEMA *via* RAFT polymerization. The number averaged molecular weights of the extended macroRAFT agents (as superscripts) as well as monomer conversions are included in the captions of the graphs. Dashed traces in case of macroRAFT^{111} (bottom left) originate from the uncontrolled polymerization region. At the bottom right, monomer conversion *versus* polymerization time is shown for chain extension of PS macroRAFT^{111} in different solvent mixtures of toluene (tol) and 1,4-dioxane (diox). As indicated, SEC traces at the bottom left originate from polymerization in toluene/1,4-dioxane = 1:3 (*v*/*v*) (Δ in monomer-conversion-*versus*-polymerization-time graph).

As solvent, varying mixtures of toluene as a good nonpolar solvent for PS and 1,4-dioxane as a good polar solvent for PMEMA were chosen. In doing so, the optimized conditions presented in the experimental section (chapter 2.1.3.) turned out. As Figure 3 depicts, a more polar solvent mixture (*i.e.* a higher 1,4-dioxane content; best results were obtained for 1,4-dioxane/toluene = 3:1 (*v*/*v*)) allows polymerization at sufficiently high rates, while a slight amount of toluene is beneficial for reduction of solvent viscosity and better dissolution of the PS macroRAFT agent. [macroRAFT]/[AIBN] is at best used in 10:1-ratio to guarantee a maximal degree of polymerization control, while a further increase was at high cost of significantly decreasing polymerization rates. The bottom left of Figure 3 shows that SEC traces shift to lower elution volume with monomer conversion (determined *via* ^{1}H NMR spectroscopy, Figure S1). In fact, this suggests an almost quantitative degree of PS end functionalization as well as a successful chain extension of the PS macroRAFT agent with a PMEMA block *via* a well-controlled RAFT mechanism. Hence, the MW distributions maintain a very narrow shape (*Đ*-values below 1.1, Table S2) up to monomer conversions of roughly 15–20%, being achieved after 15–20 h of polymerization (The longer the PS macroRAFT chain, the slower the polymerization, see also Table S2.). The well-controlled area, however, is followed by a flattening of monomer-conversion-*versus*-time plots (Figure 3, bottom right), indicating increased irreversible termination processes. Furthermore, a broadening/shouldering of the MW distributions can be observed at those time periods. This can be related to radical combination and uncontrolled chain transfer steps (Figure 3, bottom

left, dashed lines). Undesired interactions of the polar PMEMA block with the apolar SDV solid phase of the SEC column could play a role in the broadening of MW distributions, too. As a result, it can be concluded that well-defined PS-*b*-PMEMA BCPs up to remarkably high MWs of above 200 kDa could successfully be synthesized.

3.3. Self-assembly of PS-*b*-PMEMA in Bulk

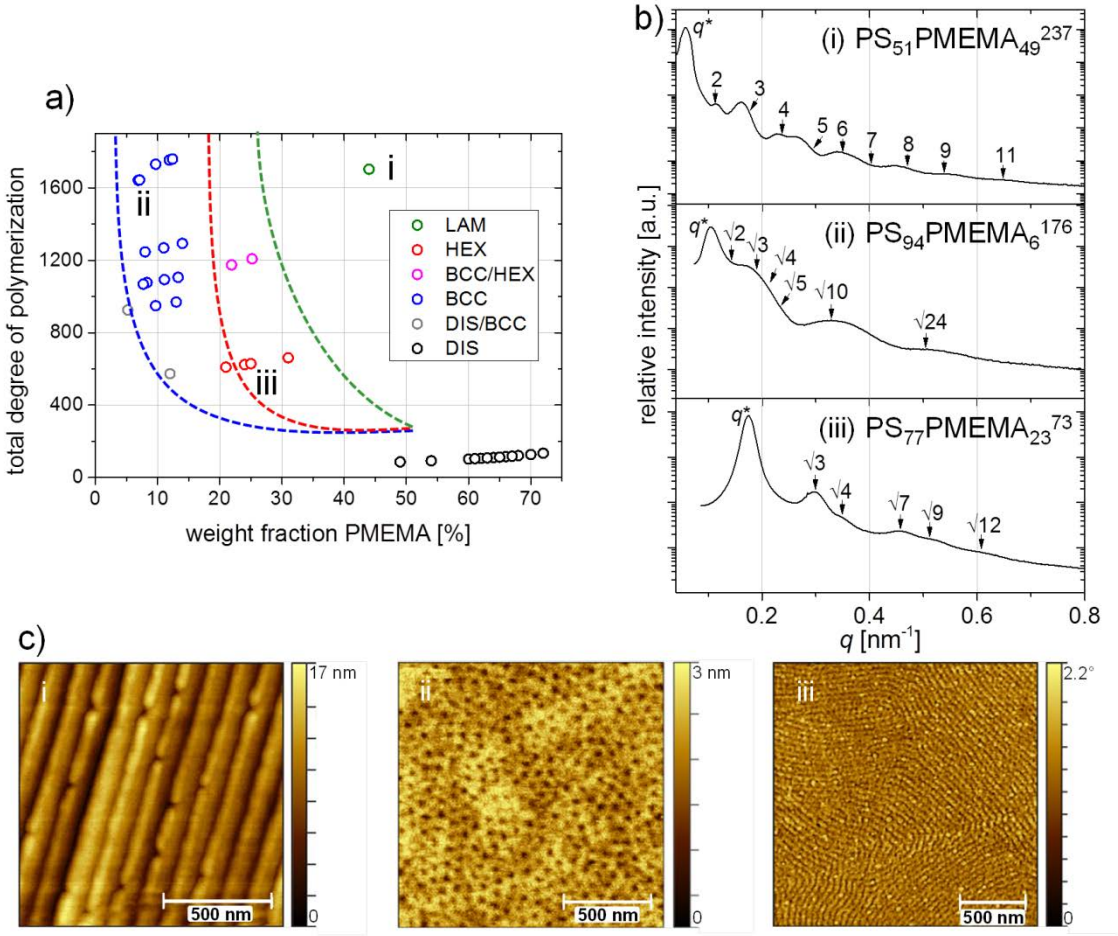

Figure 4 Bulk structures of PS-*b*-PMEMA thick films. a) Sketched phase diagram with obtained morphologies for different block copolymer compositions. i: lamellar (LAM), ii: body centered cubic (BCC), iii: hexagonal (HEX) (not shown: disordered (DIS)). b) Exemplary SAXS curves (relative scattering intensity *versus* scattering vector *q*) for different block copolymers marked in "a)". *q** indicates the first Bragg reflection, the numbers show calculated positions of peak maxima for the different structures as multiples of *q**. c) AFM surface images (height and phase image, respectively) corresponding to the depicted SAXS curves in "b)". More SAXS curves as well as AFM images can be found in the Supplementary Data.

To investigate the microphase separation of the synthesized BCPs, thick films (≈ 1 mm thickness) were produced *via* slow solvent evaporation from THF solution. The films were analyzed with SAXS to evaluate characteristic peak positioning of Bragg reflections, depending on the structure factor and, therefore, morphologies (BCC/FCC spheres, hexagonally packed cylinders, or lamellae) of the self-assembled bulk structure.[43] It shall be mentioned here that the weight fraction *f* (determined *via* ^{1}H NMR spectroscopy, see Figure S2) instead of volume fraction is used to describe the block ratio because the density ρ of the PMEMA block is unknown. In most theoretical models, though, volume fraction of the blocks is used to describe the shape of the binary phase diagram of the microphase separation. However, PMEMA density is assumed to be close to the density of the PS block (ρ = 1.05 g cm^{-3}), which is why *f* should not differ too much from volume fraction.

Besides the BCPs obtained *via* chain extension of PS macroRAFT[6], all other synthesized BCPs show multiple Bragg reflections in SAXS measurements (see Figure 4), indicating a very distinct and long-ranged degree of ordering in the bulk structure. Furthermore, as it is shown in the Supplementary Data (Figure S4), some samples even show anisotropic effects in the first order reflection, which is a sign for a very extended domain size. Figure 4a depicts sort of a phase diagram of PS-*b*-PMEMA in which the BCPs with their corresponding bulk morphology obtained *via* SAXS and AFM are included. Furthermore, exemplary SAXS patterns and AFM images of the film surfaces are shown. Lattice constants obtained from the first Bragg reflection q^* fit quite well to the one gained from the AFM images (deviation < 10%). In the following, the abbreviated notation $PS_xPMEMA_y^z$, with x being the weight fraction of the PS block, y being the weight fraction of the PMEMA block and z being the total $\overline{M}_n$-value of the BCP in kDa, is used. Microphase separated morphologies are observed already for $PS_{88}PMEMA_{12}^{64}$, which shows the strong tendency of the two blocks to segregate. This is caused in their high difference in chemical composition and, hence, polarity. Although for higher MWs of the macroRAFT agents high f-values of PMEMA are hardly achievable, which is a result of the mentioned chain growth inhibition, the phase diagram seems to have the common shape.[44]
The described results prove the presented synthesis to be a straight forward pathway to highly self-assembled materials. However, the created phase diagram is indeed not yet complete, as, besides volume fractions of the blocks, the χ parameter is unknown to date. The drawn phase boundaries are, thus, solely empirical and somewhat elusive. Nevertheless, the phase diagram might help to predict, which block ratio is needed at a specific chain length to obtain the desired bulk morphology, *e.g.* in surface patterning.

3.4. Self-assembly of PS-*b*-PMEMA in Aqueous Solution and Stimuli-responsive Micelles

When a THF solution of the BCP is added carefully to aqueous media, the BCP self-assembles into micellar structures with a PS core and a PMEMA corona, as water is a highly selective solvent for the PMEMA block. As polymer, $PS_{67}PMEMA_{33}^{166}$ was used in concentrations of 0.01 wt% (≡ 0.1 g L^{-1}). The obtained micelles own highly reproducible R_h-values of 35 nm with size dispersities of below 0.15 (as was determined *via* DLS), indicating the uniform size of the created micelles despite the very straight forward way of micelle generation by simple addition of BCP/THF solution to water and subsequent THF evaporation. The relatively small size of the micelles, in regard to the high chain length of the used polymer, suggests a highly collapsed PS core (as could be expected) and a rather coiled PMEMA corona at pH 7. It shall be mentioned at this point that the conducted rapid mixing of THF and the selective solvent water, according to literature, leads to more uniform and smaller spherical micellar structures than gradual addition of the selective solvent.[45-48] However, a vast number of different techniques for creating BCP micelles exists but that is not topic of this work.

3.4.1. Thermoresponsive Micelles

In a temperature-dependent DLS experiment, the thermoresponsive behavior of the PMEMA corona can be observed (Figure 5). As was recently reported by our group, PMEMA homopolymer shows a remarkable three-step aggregation behavior upon heating in comparable experiments.[21] In fact, in the BCP micelles a two-step aggregation behavior is preserved with a first aggregation process at 34 °C and a second cloud point (CP) at 37 °C.

The first CP, as for the PMEMA homopolymer, can be dedicated to the intramolecular coil-to-globule transition of the single PMEMA chains in the corona followed by a first aggregation process, being interrupted by surface hydration of the formed aggregates (which are still remarkably uniform in size). At the second CP, aggregate hydration collapses, macroscopic aggregates form and sedimentate. Both phase transitions are sharp, especially at CP2. This is indeed remarkable, because it suggests a high degree of cooperativity of the H-bond cleavage in between water and the aggregate surface, which is usually only the case if intramolecular H-bonds can be formed (*e.g.* in poly[*N*-isopropylacrylamide] (PNIPAm)).[49,50] The observed cooperativity can be assigned to the spatial proximity of the collapsing PMEMA chains in the micelle corona and aggregate surface, respectively, *i.e.* the coil-to-globule transition of one chain affects its neighbors. Certainly, the sharpness of temperature-induced phase transitions is also a matter of heating rate, which is very low in our DLS experiments ($dT/dt \approx 2$ °C h^{-1}). This also makes us believe that the described aggregate structures are indeed close to thermodynamic equilibrium. Due to the high apparent degree of micelle aggregation and entanglements, though, both aggregation steps appear to be irreversible on the time scale of the conducted temperature ramp. Actually, the precipitate formed at the second CP was stable for weeks at room temperature, showing the enormous kinetic inhibition of redissolution of the aggregates.

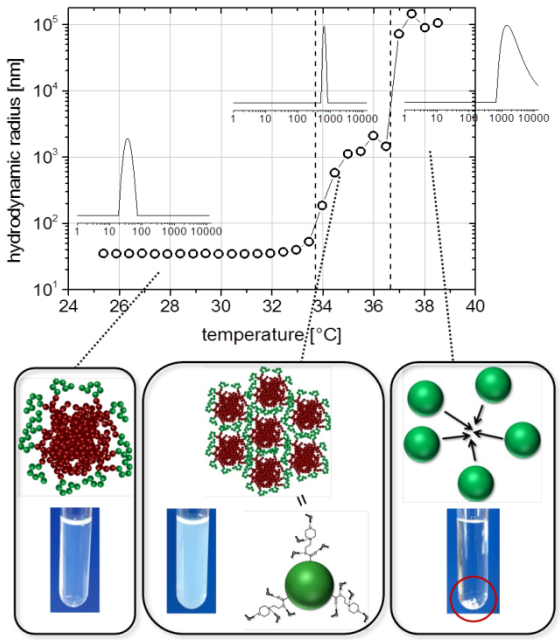

Figure 5 Hydrodynamic radius *versus* temperature for an aqueous micellar solution of $PS_{67}PMEMA_{33}^{166}$ ([BCP] = 0.1 wt%) at pH 7. In the insets, exemplary size distributions (*x*-axis: hydrodynamic radius in nm) obtained *via* fitting with a CONTIN algorithm are shown. The drawings at the bottom give interpretations for the different observed aggregate structures.

3.4.2. pH-responsive Micelles

As was mentioned in the introduction section, morpholino units in the PMEMA side chains react as base with a pK_a-value of the conjugated acid at around 4.9.[22] If the morpholino nitrogen is protonated at low pH, the charged PMEMA chains are more hydrophilic than in the neutral state, leading to a significant increase of the CP out of the experimentally achievable range. Indeed, at pH 2 the BCP micelles show a higher, still very uniform R_h-value of 72 nm (see inset of Figure 6). This value fits exceptionally well to a theoretically calculated

one under the assumption of a fully collapsed PS block in the core, *i.e.* each PS block forms a dense globule, and a completely stretched PMEMA corona in all-trans conformation:

$$R_{\mathrm{h,micelle}} = d_{\mathrm{PS,collapsed}} + d_{\mathrm{PMEMA,all\text{-}trans}} = 2 \times \underbrace{\sqrt[3]{\frac{3\times\overline{M}_{\mathrm{n,PS}}}{4\times\pi\times N_{\mathrm{A}}\times\rho_{\mathrm{PS}}}}}_{\approx 7\ \mathrm{nm}} + \underbrace{P_{\mathrm{PMEMA}} \times l_{\mathrm{PMEMA}}}_{\approx 58\ \mathrm{nm}} \approx 72\ \mathrm{nm}. \quad (2)$$

d_i: diameter of block i. ρ_{PS}: density of amorphous PS (≈ 1.05 g L^{-1}). N_A: Avogadro constant. P_{PMEMA}: polymerization degree of PMEMA block. l_{PMEMA}: effective backbone length of one repeating unit ($l_{PMEMA} \approx 0.25$ nm).

The stretching of the PMEMA corona is necessary due to repulsive interactions of the almost fully protonated and therefore identically charged morpholino units, which leads to a sea-urchin-like shape of the micelles (Figure 6). Furthermore, the protonated PMEMA chains are expected to be highly hydrated and, indeed, show no CP up to 70 °C. The assumption of an amorphous spherical PS micelle core with a radius of 14 nm according to Equation 2 can also be used to roughly estimate an aggregation number N_{agg}, which gives a value of $N_{agg} \approx 65$. In fact, this is by a factor of approximately 3 lower than reported N_{agg} for PS core micelles from BCPs with comparable PS block lengths.[51] Though, this work dealed with crew-cut micelles owning a very short hydrophilic block with much less effective volume than the PMEMA block in our case. As Eisenberg *et al.* discussed, increasing coil dimensions of the corona forming block with higher polymerization degree decrease N_{agg} due to repulsive interchain interactions.[15] Furthermore, the fast mixing of THF and water for micelle preparation generates smaller nucleation and self-assembly seeds than by gradual water addition conducted in the mentioned work.[46,48] Thus, the observed lower N_{agg} appears reasonable to us.

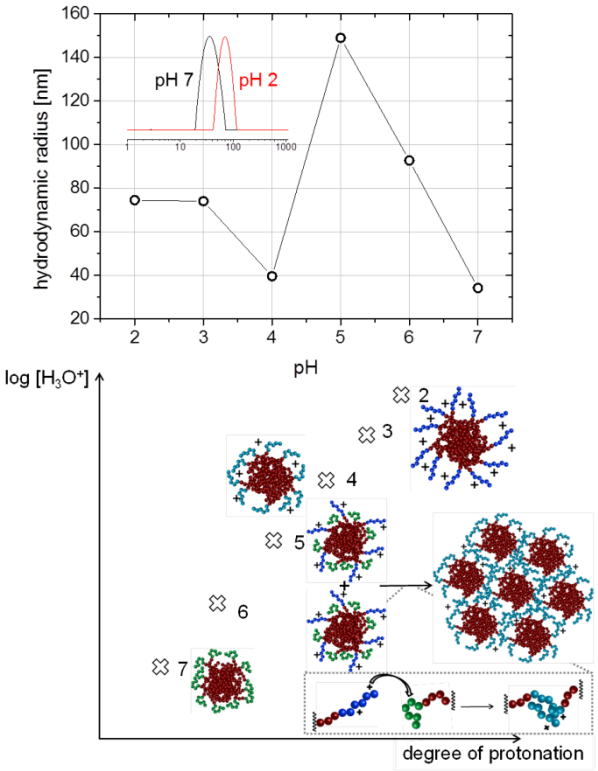

Figure 6 Hydrodynamic radius *versus* pH-value (top) of an aqueous micellar solution of $PS_{67}PMEMA_{33}^{166}$. The inset shows two exemplary size distributions (*x*-axis: hydrodynamic radius in nm) at pH 7 (black) and pH 2 (red) obtained *via* fitting with a CONTIN algorithm (for further size distributions see Figure S5). The cartoon at the bottom gives an explanation hypothesis of the observed aggregated structures (numbers in the graph indicate pH-value). Green chains in the corona indicate an unprotonated state, blue chains a highly protonated state, turquoise chains a medium protonation degree.

At slightly acidic pH, *i.e.* pH 6 and pH 5, a peculiar observation can be made: R_h-values of the aggregates become surprisingly high ($R_h > 100$ nm) and size distributions get very broad (Figure 6, top, and Figure S5). As was further evaluated at pH 5, particle radii increase with time after acid addition (from 35 nm to 180 nm within 20 h, Figure S5), which suggests slow micelle combination in case of partial protonation of the corona. Our explanation of this phenomenon is still somewhat elusive. However, it is known from BCP blends that if a stretched chain with low degree of entropical freedom and a more coiled chain with higher entropical freedom interpenetrate, both chains adopt a conformation with medium degree of stretching.[52,53] By this, the gain of entropy of the formerly highly stretched chain overcompensates the entropy loss of the formerly coiled chain. Transferring this model to the case of a partially protonated micelle corona in a sense that some chains are more protonated/stretched than others, micelle combination will result *via* intermicellar PMEMA entanglements. By the correlated proton exchange, entangled chains obtain a similar degree of protonation and stretching (Figure 6, bottom). This would explain the aggregate growth with time. If all PMEMA chains in the micelle corona obtain a significantly high degree of protonation, as it is the case at pH 4 ($[H_3O^+] \approx$ [MEMA units]), entanglements are not beneficial anymore. In addition, identical charges and a high hydration degree of the corona prevents micelle combination which is why much lower R_h-values of 40 nm are observed at pH 4 than at pH 6 and 5. At pH 3 as well as at pH 2, the maximal degree of protonation is achieved and micelles adopt the sea-urchin shape with their maximal size of roughly 70 nm.

3.4.3. Salt-responsive Micelles

Having in mind that there is currently an ongoing highly vivid debate about the origin of salting-in and salting-out effects of ions on hydrophobic solutes,[54] salt-responsivity is a mechanistically interesting and potentially useful tuning feature of water soluble polymers. Because human blood plasma contains significant amounts of salts (mainly NaCl in roughly 0.1 M concentration), knowledge of salt influence is also crucial when discussing a potential application of stimuli-responsive BCPs as drug delivery systems. This is why salt-response of the BCP micelles was exemplary evaluated by addition of NaCl and NaBr, respectively, to the micellar BCP solutions (Figure 7). While Cl^- is a weak kosmotropic anion according to the Hofmeister series, meaning that it owns a rather high charge density and, thus, increases solvent surface tension in the inner hydration shell of a polymer, Br^- is known to be a chaotropic anion. Chaotropes, simply spoken, disturb the originally well-ordered water structure and therefore enable more water to hydrate a solute.[55-57] Additionally, chaotropic ions can directly adsorb to a dissolved polymer, resulting in a surface charge. Hence, the addition of chaotropes to polymer solutions leads to a salting-in effect and a CP-*versus*-anion-concentration curve shows a shape comparable to a Langmuir isotherm.[56] On the other hand, addition of kosmotropes induces a salting-out effect, and this effect increases proportionally with kosmotrope concentration.

Indeed, the described trends are observed in our CP experiments under salt addition in case of CP1, while the effect is much more pronounced for NaBr than for NaCl (Figure 7). By NaBr addition, CP1 and CP2 are increased in a similar manner, suggesting that micelles as well as aggregates formed above CP1 are equally stabilized by adsorption of the Br^-. It can also be stated that Br^- adsorption on the polymer is more favored than Br^- hydration by water molecules, which, for itself, would result in a CP decrease.

Surprisingly, while being a kosmotrope for PMEMA homopolymer,[21] the addition of Cl^- to the micellar solution leads to a Langmuir-shaped increase of CP2. This indicates that towards the formed aggregates above CP1, Cl^- rather acts as chaotrope than as kosmotrope. Often, the weak ordering effect of Cl^- on the water network structure causes a slight salting-out effect

and that is indeed observed as a slight CP decrease in case of CP1. However, Cl^- ions are polarizable to a certain extent, which is why the kosmotropic effect is certainly superimposed by chaotrope-like adsorption on the micelle surface. This goes well with reports in which a chaotropic behavior of Cl^- is described, depending pretty much on counter ion and interaction partner.[58] When the micelle surface area is decreased *via* aggregate formation above CP1, the relative concentration of Cl^- increases (because a comparable number of Cl^- anions is unhydrated and therefore available for adsorption), *i.e.* a higher degree of aggregate surface is stabilized *via* anion adsorption compared to the micelles. Thus, a chaotropic behavior of Cl^- is observed above CP1.
To conclude, the results clearly image the salt-responsivity of the PMEMA micelle corona. The collapse of the micellar system can be tuned *via* salt addition in both directions, *i.e.* CPs can be shifted to lower temperatures by addition of salts being on the left of Cl^- in the Hofmeister rowing (*e.g.* SO_4^{2-}, CO_3^{2-}, F^-). If a CP increase is desired, anions like Br^-, I^- or SCN^- might be added.

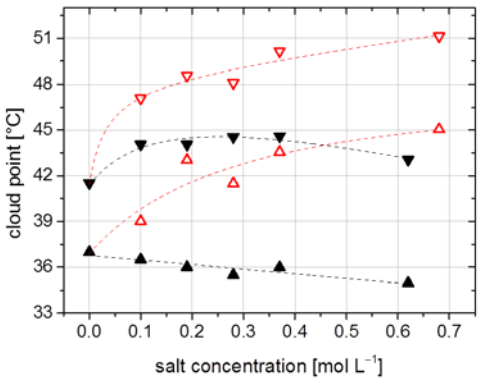

Figure 7 Cloud points *versus* salt concentration for an aqueous micellar solution of $PS_{67}PMEMA_{33}^{166}$ at pH 7 under addition of NaBr (red) and NaCl (black), respectively. Δ indicates the first cloud point (see Figure 5), ∇ the second cloud point. The fits are supposed to guide the eye.

3.4.4. Influence of Solvent-to-Water Ratio on Micelle Size

A common way to produce BCP micelles is the exchange of a good solvent for both blocks, *e.g.* THF or 1,4-dioxane, by a selective solvent for one of the blocks, in this case water.[15] To simulate the mechanistic pathway of micelle formation *via* this procedure, different amounts of water were added to a solution of the BCP in THF and 1,4-dioxane ([BCP] = 0.05 wt%), respectively (Figure 8, for size distributions see Figure S6 and S7). By this method, the ratio of organic solvent to water at which the PS block collapses and forms the micelle core, the so-called critical water content (CWC), can be obtained.
The CWC is observable by a jump in R_h-value from below 15 nm for the dissolved random polymer coil to 60 nm in 1,4-dioxane/water (CWC = 10 vol%) and roughly 100 nm in THF/water (CWC = 14 vol%), respectively. Those values are higher than R_h of the micelles in pure water (≈ 35 nm) due to the swelling of the polymer, especially of the PS core, with the organic solvent and therefore a looser packing at lower water contents.[51] According to that, a deswelling of the micelle core at higher water contents can be expected, which was actually observed in case of 1,4-dioxane/water mixtures (Figure 8, red circles).
In case of THF/water, a slight deswelling of the PS core from 14 vol% water content to 30 vol% is followed by an increase in R_h with higher water contents up to a maximum of 180 nm at a water content of 85 vol% (Figure 8, black squares). As was reviewed for instance by Mai and Eisenberg, the water content influences the aggregation number as well as micelle

shape, as it may change from spheres to rods to vesicles with increasing water content.[15] With higher aggregation number at higher water contents, the PS chains in the micelle core become more stretched, which would explain the higher R_h-values. Also, shapes as rods or vesicles own higher R_h-values than spherical micelles. However, because size distributions appear to be very narrow over the whole range of solvent compositions (see Figure S6), non-spherical anisotropic shapes like rods can be excluded. As mentioned above, the addition rate of the selective solvent also has a pronounced effect on the formed micellar structures, while we conducted solely a rapid mixing of solvent and water in this work.[45]

Another interesting explanation attempt can be made from the observation that aggregated structures are also observed for PMEMA homopolymer (Figure S8) under similar conditions. This suggests that the PMEMA corona is destabilized in THF/water mixtures with water contents of 30 to 95 vol%, and the R_h-increase goes back to micelle aggregation. The highly interesting phenomenon that two good solvents for a polymer give a bad solvent in mixtures of the two is called cononsolvency.[59] It is mostly reported for aqueous polymer solutions, often PNIPAm, under addition of alcohols.[50,60-62] In the past few years, cononsolvency gained a lot of interest in the scientific community due to the fact that it allows detailed insights into water structures and their hydration behavior. However, understanding of the cononsolvency effect appears to be very complex and different opinions about the origin of the effect exist (whether it can be dedicated preferentially to additive/water or additive/polymer interactions).[60,63,64] We suggest the following explanation for our reported example:

When the water content is high, THF molecules are preferentially hydrated, *i.e.* less water is available to hydrate the PMEMA corona; the formed micelles aggregate to a certain extent (water content of 100 to 85 vol%). At lower water contents, some THF molecules remain unhydrated and, by this, are available to solvate the micellar structures generated by water addition; aggregation degree and R_h-value shrink (water content of 85 to 30 vol%). With higher proximity of the THF/water ratio to the CWC, the cononsolvency effect becomes negligible. The PS core of the in this stage single micelles swells with higher THF content (water content of 30 to 14 vol%), until micelle formation is prevented due to effective solvation of the PS block by THF molecules (water content of 14 to 0 vol%).

Because those reported findings appear peculiar and interesting to us, further related experiments are currently in progress. For instance, other organic additives with different chemical structures as well as with lower volatility can be investigated. This might allow temperature-dependent measurements, as evaporation of the rather volatile THF at elevated temperatures cannot be excluded in our current experimental DLS setup. In case of an actual cononsolvency effect, CPs should decrease compared to pure water. Furthermore, the rate of water addition to the BCP/solvent mixtures can be varied to verify thermodynamic and kinetic effects. In addition, as was presented recently by Pochan *et al.*, the water addition rate can strongly influence size and shape of created nanoparticles, making it a versatile tool to design tailored micellar structures.[46]

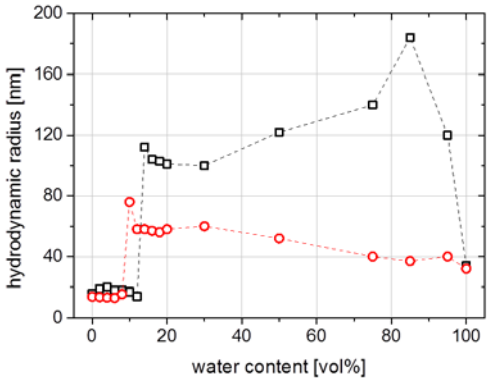

Figure 8 Hydrodynamic radius *versus* relative water content of $PS_{67}PMEMA_{33}^{166}$ micelles/aggregates in solvent mixtures of THF/water (□) and 1,4-dioxane/water (○), respectively. For size distributions, see Figure S6 and S7.

4. Conclusion

In this work, a versatile way to high MW PS-*b*-PMEMA BCPs is described. The combination of anionic polymerization for the major, hydrophobic PS block and RAFT polymerization for the minor, hydrophilic and stimuli-responsive PMEMA block allows the synthesis of BCPs with very narrow MW distributions. To the best of our knowledge, achieved MWs are some of the highest reported so far for BCPs being synthesized *via* the presented combination pathway (and by far higher than MWs being achievable *via* pure sequential CRP). Therefore, the presented synthesis proves to be useful for making polymers which are suitable for applications in which mechanically robust (due to enhanced entanglements through high chain length) self-organizing (high block repulsion) materials are needed. In addition, as a result of the high functional group tolerance of the RAFT process, the minor block can be chemically tailored for the desired purpose. In our example, the utilized PMEMA block shows responsivity towards multiple stimuli, which could be interesting for switchable self-assembled materials, *e.g.* drug delivery systems or chemical valves. For instance, a load implemented into the PS core of PS-*b*-PMEMA micelles can be effectively shielded by the PMEMA corona at low pH, independently of temperature. At neutral pH, the load might easily be released by increasing the temperature just slightly above room temperature. Added salts can further tune the temperature-induced collapse of the micelle corona both upwards and downwards in temperature. Additionally, from a more mechanistic point of view, findings such as a two-step micelle aggregation process upon heating, a non-trivial micelle behavior at slightly acidic pH, kosmotropy and chaotropy of the used salts as well as an observed potential cononsolvency effect in polymer/THF/water mixtures tackle currently discussed aspects in stimuli-responsive polymer science.

Acknowledgements

S.E. gratefully acknowledges financial support of the Fonds der Chemischen Industrie (FCI). Dr. Andreas Meyer is thanked for his help with the SAXS measurements, Dr. Doreen Alisch for helping with the synthesis of first PS–OH samples.

Author Contributions

The manuscript was written through contributions of all authors. All authors have given approval to the final version of the manuscript. The authors declare no competing financial interest.

Appendix A. Supplementary Data

Supplementary data related to this article can be found at…

References

[1] Braunecker WA, Matyjaszewski K. Prog Polym Sci 2007;32(1):93-146.
[2] Georges MK, Veregin RPN, Kazmaier PM, Hamer GK. Macromolecules 1993;26(11):2987-2988.
[3] Kato M, Kamigaito M, Sawamoto M, Higashimura T. Macromolecules 1995;28(5):1721-1723.
[4] Wang J-S, Matyjaszewski K. J Am Chem Soc 1995;117(20):5614-5615.
[5] Chiefari J, Chong YK, Ercole F, Krstina J, Jeffery J, Le TPT, Mayadunne RTA, Meijs GF, Moad CL, Moad G, Rizzardo E, Thang SH. Macromolecules 1998;31(16):5559-5562.
[6] Galaev I, Mattiasson B. Smart Polymers – Applications in Biotechnology and Biomedicine, 2 ed. Boca Raton: CRC Press, 2008.
[7] Cabane E, Zhang XY, Langowska K, Palivan CG, Meier W. Biointerphases 2012;7(1-4).
[8] Abetz V. Macromol Rapid Commun 2015;36(1):10-22.
[9] Sai H, Tan KW, Hur K, Asenath-Smith E, Hovden R, Jiang Y, Riccio M, Muller DA, Elser V, Estroff LA, Gruner SM, Wiesner U. Science 2013;341(6145):530-534.
[10] Schacher FH, Rupar PA, Manners I. Angew Chem Int Edit 2012;51(32):7898-7921.
[11] Priya James H, John R, Alex A, Anoop KR. Acta Pharm Sin B 2014;4(2):120-127.
[12] Bates FS, Fredrickson GH. Phys Today 1999;52(2):32-38.
[13] Blanazs A, Armes SP, Ryan AJ. Macromol Rapid Commun 2009;30(4-5):267-277.
[14] Groschel AH, Walther A, Löbling TI, Schacher FH, Schmalz H, Müller AHE. Nature 2013;503(7475):247-251.
[15] Mai YY, Eisenberg A. Chem Soc Rev 2012;41(18):5969-5985.
[16] Walker JS, Vause CA. Scientific American 1987;256(5):98-105.
[17] Deshmukh SA, Sankaranarayanan SKRS, Suthar K, Mancini DC. J Phys Chem B 2012;116(9):2651-2663.
[18] Smith AE, Xu XW, Kirkland-York SE, Savin DA, McCormick CL. Macromolecules 2010;43(3):1210-1217.
[19] Wang D, Wu T, Wan X, Wang X, Liu S. Langmuir 2007;23(23):11866-11874.
[20] Wang D, Yin J, Zhu Z, Ge Z, Liu H, Armes SP, Liu S. Macromolecules 2006;39(21):7378-7385.
[21] Eggers S, Fischer B, Abetz V. Macromol Chem Phys 2016;217(6):735-747.
[22] Bütün V, Armes SP, Billingham NC, Tuzar Z, Rankin A, Eastoe J, Heenan RK. Macromolecules 2001;34(5):1503-1511.
[23] Bütün V, Armes SP, Billingham NC. Polymer 2001;42(14):5993-6008.
[24] Van Overstraeten-Schlogel N, Shim YH, Tevel V, Piel G, Piette J, Dubois P, Raes M. Drug Delivery 2012;19(2):112-122.

[25] Reschner A, Shim YH, Dubois P, Delvenne P, Evrard B, Marcelis L, Moucheron C, Kirsch-De Mesmaeker A, Defrancq E, Raes M, Piette J, Collard L, Piel G. J Biomed Nanotechnol 2013;9(8):1432-1440.
[26] Szwarc M. Nature 1956;178(4543):1168-1169.
[27] Smith AE, Xu XW, McCormick CL. Prog Polym Sci 2010;35(1-2):45-93.
[28] Chapman R, Gormley AJ, Herpoldt KL, Stevens MM. Macromolecules 2014;47(24):8541-8547.
[29] Xu JT, Shanmugam S, Duong HT, Boyer C. Polym Chem-Uk 2015;6(31):5615-5624.
[30] Shanmugam S, Xu JT, Boyer C. Macromolecules 2014;47(15):4930-4942.
[31] Xu JT, Jung K, Atme A, Shanmugam S, Boyer C. J Am Chem Soc 2014;136(14):5508-5519.
[32] Hill MR, Carmean RN, Sumerlin BS. Macromolecules 2015;48(16):5459-5469.
[33] Yin LG, Dalsin MC, Sizovs A, Reineke TM, Hillmyer MA. Macromolecules 2012;45(10):4322-4332.
[34] Schmidt BVKJ, Elbert J, Barner-Kowollik C, Gallei M. Macromol Rapid Commun 2014;35(7):708-714.
[35] Pafiti KS, Patrickios CS, Filiz V, Rangou S, Abetz C, Abetz V. J Polym Sci, Part A: Polym Chem 2013;51(1):213-221.
[36] Zhang C, Yang YL, He JP. Macromolecules 2013;46(10):3985-3994.
[37] Förster S, Krämer E. Macromolecules 1999;32(8):2783-2785.
[38] Quirk RP, Pickel DL, Hasegawa H. Macromol Symp 2005;226(1):69-78.
[39] Quirk RP, Hasegawa H, Gomochak DL, Wesdemiotis C, Wollyung K. Macromolecules 2004;37(19):7146-7155.
[40] Quirk RP, Lizarraga GM. Macromolecules 1998;31(11):3424-3430.
[41] Nayak JN, Aralaguppi MI, Naidu BVK, Aminabhavi TM. J Chem Eng Data 2004;49(3):468-474.
[42] Olaj OF, Vana P, Zoder M. Macromolecules 2002;35(4):1208-1214.
[43] Hamley IW, Castelletto V. Prog Polym Sci 2004;29(9):909-948.
[44] Matsen MW, Bates FS. Macromolecules 1996;29(4):1091-1098.
[45] Hayward RC, Pochan DJ. Macromolecules 2010;43(8):3577-3584.
[46] Chen YC, Zhang K, Wang XJ, Zhang FW, Zhu JH, Mays JW, Wooley KL, Pochan DJ. Macromolecules 2015;48(16):5621-5631.
[47] Hauschild S, Lipprandt U, Rumplecker A, Borchert U, Rank A, Schubert R, Förster S. Small 2005;1(12):1177-1180.
[48] Cui HG, Chen ZY, Wooley KL, Pochan DJ. Soft Matter 2009;5(6):1269-1278.
[49] Maeda Y, Nakamura T, Ikeda I. Macromolecules 2002;35(27):10172-10177.
[50] Scherzinger C, Balaceanu A, Hofmann CH, Schwarz A, Leonhard K, Pich A, Richtering W. Polymer 2015;62:50-59.
[51] Gao ZS, Varshney SK, Wong S, Eisenberg A. Macromolecules 1994;27(26):7923-7927.
[52] Goldacker T, Abetz V, Stadler R, Erukhimovich I, Leibler L. Nature 1999;398(6723):137-139.
[53] Leibler L, Gay C, Erukhimovich I. Europhys Lett 1999;46(4):549-554.
[54] Ball P, Hallsworth JE. PCCP 2015;17(13):8297-8305.
[55] Kunz W, Henle J, Ninham BW. Curr Opin Colloid Interface Sci 2004;9(1-2):19-37.
[56] Zhang YJ, Furyk S, Bergbreiter DE, Cremer PS. J Am Chem Soc 2005;127(41):14505-14510.
[57] Zhang Y, Furyk S, Sagle LB, Cho Y, Bergbreiter DE, Cremer PS. The Journal of Physical Chemistry C 2007;111(25):8916-8924.
[58] Collins KD. P Natl Acad Sci USA 1995;92(12):5553-5557.

[59] IUPAC. Compendium of Chemical Terminology, 2 ed. Oxford: Blackwell Scientific Publications, 1997.
[60] Costa ROR, Freitas RFS. Polymer 2002;43(22):5879-5885.
[61] Ebeling B, Eggers S, Hendrich M, Nitschke A, Vana P. Macromolecules 2014;47(4):1462-1469.
[62] Scherzinger C, Schwarz A, Bardow A, Leonhard K, Richtering W. Curr Opin Colloid Interface Sci 2014;19(2):84-94.
[63] Kyriakos K, Philipp M, Adelsberger J, Jaksch S, Berezkin AV, Lugo DM, Richtering W, Grillo I, Miasnikova A, Laschewsky A, Müller-Buschbaum P, Papadakis CM. Macromolecules 2014;47(19):6867-6879.
[64] Schild HG, Muthukumar M, Tirrell DA. Macromolecules 1991;24(4):948-952.

SUPPLEMENTARY DATA

Synthesis and Self-Assembly of High Molecular Weight Polystyrene-*block*-poly[2-(*N*-morpholino)ethyl methacrylate]: A Story about Microphase Separation, Amphiphilicity, and Stimuli-responsivity

Steffen Eggers, Felix Lauterbach, Volker Abetz*

^{1}H NMR Spectra for Determination of Monomer Conversion and Block Copolymer Composition

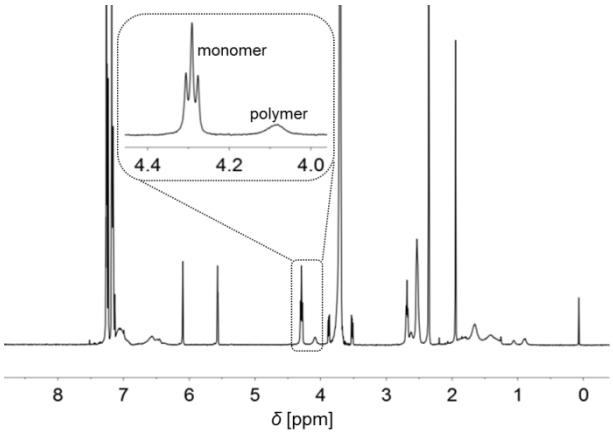

Figure S1 Typical ^{1}H NMR spectrum of a polymerization mixture in the chain extension of a polystyrene macroRAFT agent with 2-(*N*-morpholino)ethyl methacrylate (MEMA) *via* RAFT polymerization. The inset shows the MEMA monomer peak (–C(O)OC*H*$_2$CH$_2$–) and related polymer peak used for calculation of monomer conversion (see Table S2).

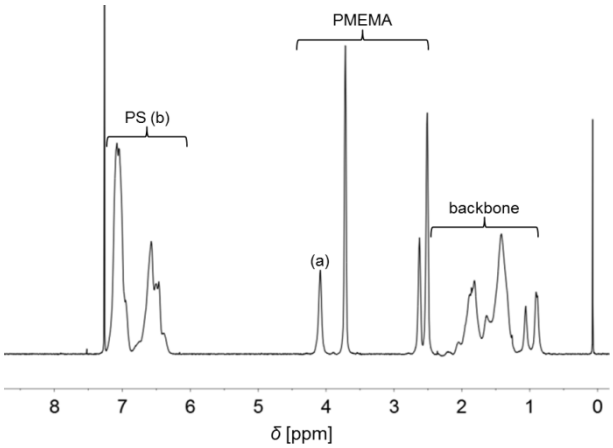

Figure S2 ^{1}H NMR spectrum of a dry block copolymer sample of polystyrene-*block*-poly[2-(*N*-morpholino)ethyl methacrylate] (PS-*b*-PMEMA). Peak (a) of the PMEMA signals (see Figure S1) and the aromatic polystyrene signals (b) were used to calculate weight fractions and molecular weights (see Table S2).

GPC Traces

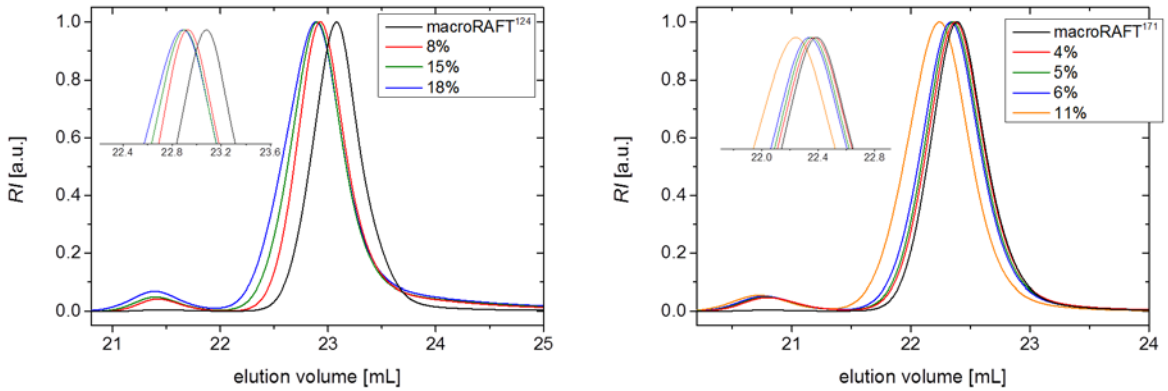

Figure S3 SEC traces (relative signal intensity (*RI*) *versus* elution volume) of block copolymers gained by chain extension of polystyrene macroRAFT agents with MEMA *via* RAFT polymerization. The number averaged molecular weights of the extended macroRAFT agents as well as monomer conversions are included in the captions of the graphs.

2D SAXS Image

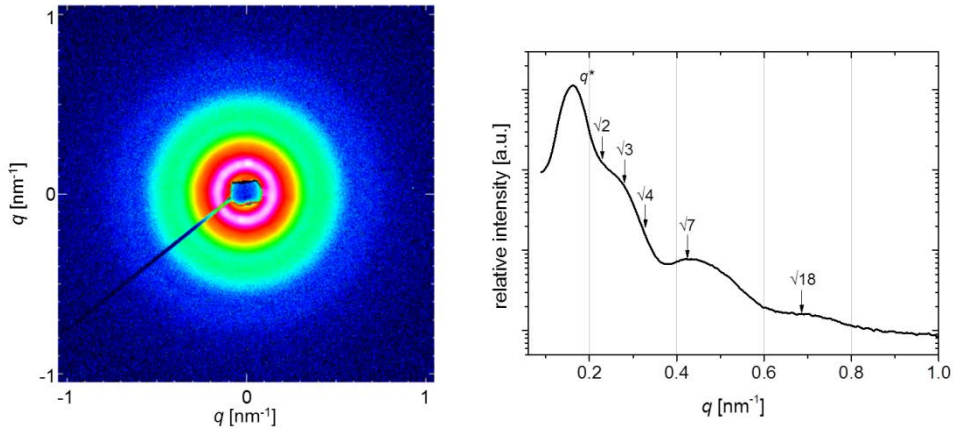

Figure S4 Two-dimensional (left) and one-dimensional (right) SAXS image of a bulk structure of $PS_{90}PMEMA_{10}^{104}$. In the two-dimensional image, the first-order reflection *q** (purple ring) appears to be anisotropic, as it can be seen by the different colors in the ring. The numbers in the one-dimensional image indicate calculated Bragg maxima for a body centered cubic (BCC) structure as multiples of *q**.

Analytical Data of the Created macroRAFT Agents

Table S1 Sample codes, number averaged molecular weights ($\overline{M}_n$) and dispersities ($Đ = \frac{\overline{M}_w}{\overline{M}_n}$) of the synthesized polystyrene macroRAFT agents *via* anionic polymerization, hydroxyl end capping with propylene oxide and subsequent Steglich esterification with a carboxyl containing RAFT agent.

Sample Code	$\overline{M}_n$ [kDa]	*Đ*
$macroRAFT^{6}$	5.6	1.26
$macroRAFT^{56}$	56	1.04
$macroRAFT^{111}$	111	1.02
$macroRAFT^{124}$	124	1.02
$macroRAFT^{171}$	171	1.02

Table S2 Exemplary analytical data of a series of PS-*b*-PMEMA block copolymers synthesized under usage of polystyrene macroRAFT agents of different chain lengths. $\overline{M}_n$: number averaged molecular weight. *f*: weight fraction of PMEMA block. *Đ*: dispersity, $Đ = \frac{\overline{M}_w}{\overline{M}_n}$.

Sample Code	$\overline{M}_{n,macroRAFT}$ [a] [kDa]	Polymerization Time [h]	Monomer Conversion [b] [%]	$\overline{M}_{n,th}$ [c] [kDa]	$\overline{M}_{n,NMR}$ [d] [kDa]	f_{PMEMA} [d] [wt%]	$\overline{M}_{n,SEC}$ [a] [kDa]	$Đ$ [a]
$PS_{39}PMEMA_{61}^{15}$	5.6	18 [e),g)]	40	13.5	15.1	61	12.0	1.18
$PS_{36}PMEMA_{64}^{16}$		24 [e),g)]	44	14.3	16.3	64	12.6	1.19
$PS_{31}PMEMA_{69}^{19}$		38 [e),g)]	57	16.9	18.8	69	13.7	1.21
$PS_{88}PMEMA_{12}^{64}$	56	18 [e),h)]	12	63	64	12	62	1.05
$PS_{86}PMEMA_{14}^{65}$		24 [e),h)]	16	65	65	14	63	1.07
$PS_{77}PMEMA_{23}^{73}$		40 [e),h)]	34	75	73	23	69	1.06
$PS_{93}PMEMA_{7}^{119}$	111	3 [f),g)]	2	114	119	7	114	1.03
$PS_{89}PMEMA_{11}^{124}$		6 [f),g)]	4	118	124	11	118	1.03
$PS_{80}PMEMA_{20}^{138}$		14 [f),g)]	11	137	138	20	123	1.04
$PS_{70}PMEMA_{30}^{158}$		20 [f),g)]	16	152	158	30	130	1.06
$PS_{67}PMEMA_{33}^{166}$		48 [f),g)]	18	158	166	33	130	1.06
$PS_{93}PMEMA_{7}^{133}$	124	24 [e),h)]	8	133	133	7	126	1.07
$PS_{86}PMEMA_{14}^{138}$		38 [e),h)]	15	140	138	14	128	1.08
$PS_{83}PMEMA_{17}^{143}$		48 [e),h)]	18	145	143	17	140	1.07
$PS_{95}PMEMA_{5}^{174}$	171	24 [e),i)]	4	172	174	5	174	1.05
$PS_{94}PMEMA_{6}^{176}$		38 [e),i)]	5	173	176	6	176	1.05
$PS_{92}PMEMA_{8}^{179}$		48 [e),i)]	6	175	179	8	179	1.05
$PS_{90}PMEMA_{10}^{190}$		24 [f),i)]	11	190	190	10	191	1.05
$PS_{88}PMEMA_{12}^{195}$		48 [f),i)]	12	191	195	12	190	1.05
$PS_{87}PMEMA_{13}^{196}$		72 [f),i)]	14	195	196	13	186	1.05

a) Determined *via* SEC in THF using PS calibration. b) Determined *via* ^{1}H NMR spectroscopy from integral ratio of MEMA monomer signal (δ = 4.28 ppm) and PMEMA polymer signal (δ = 4.05 ppm) (see Figure S1). c) $\overline{M}_{n,th} = \frac{[MEMA]}{[macroRAFT]} \times M_{MEMA} \times$ monomer conversion $+ \overline{M}_{n,macroRAFT}$. d) Determined *via* ^{1}H NMR spectroscopy from integral ratio of PS signal at δ = 7.31–6.29 ppm and PMEMA signal at δ = 4.05 ppm under usage of $\overline{M}_{n,macroRAFT}$ (see Figure S2). e) Synthesized at 60 °C. f) Synthesized at 65 °C. g) [macroRAFT]/[AIBN] = 10:1. h) [macroRAFT]/[AIBN] = 5:1. i) [macroRAFT]/[AIBN] = 7:1.

SAXS and AFM Images

$PS_{51}PMEMA_{49}^{237}$

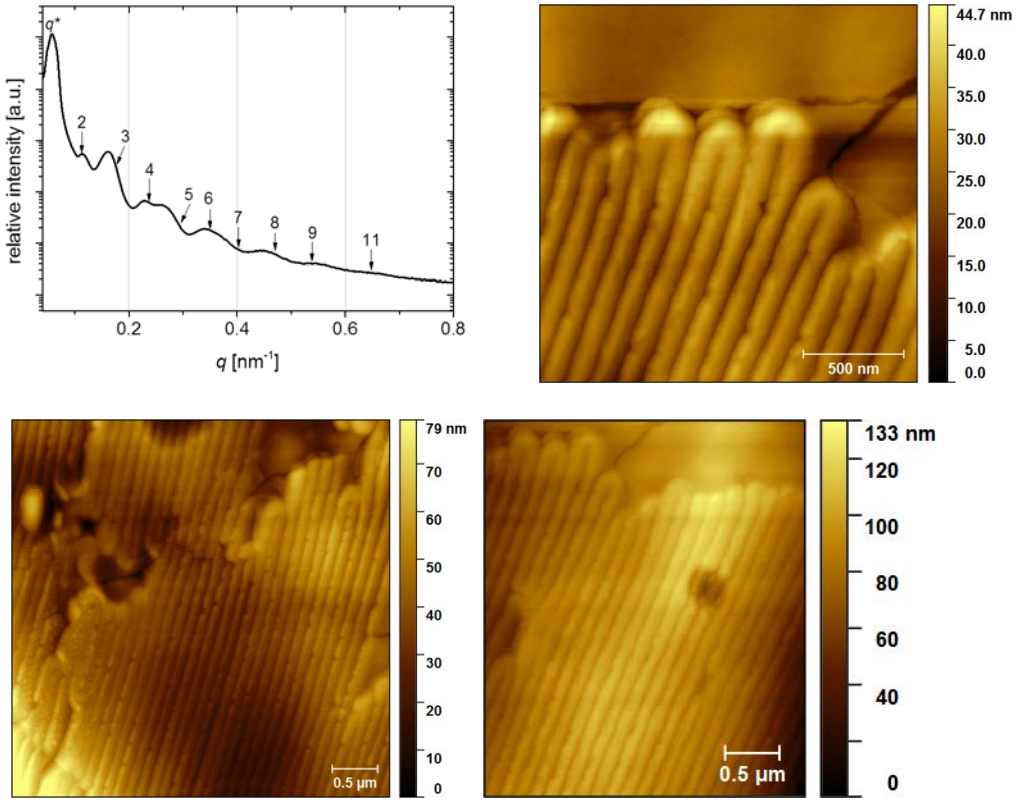

$PS_{88}PMEMA_{12}^{195}$

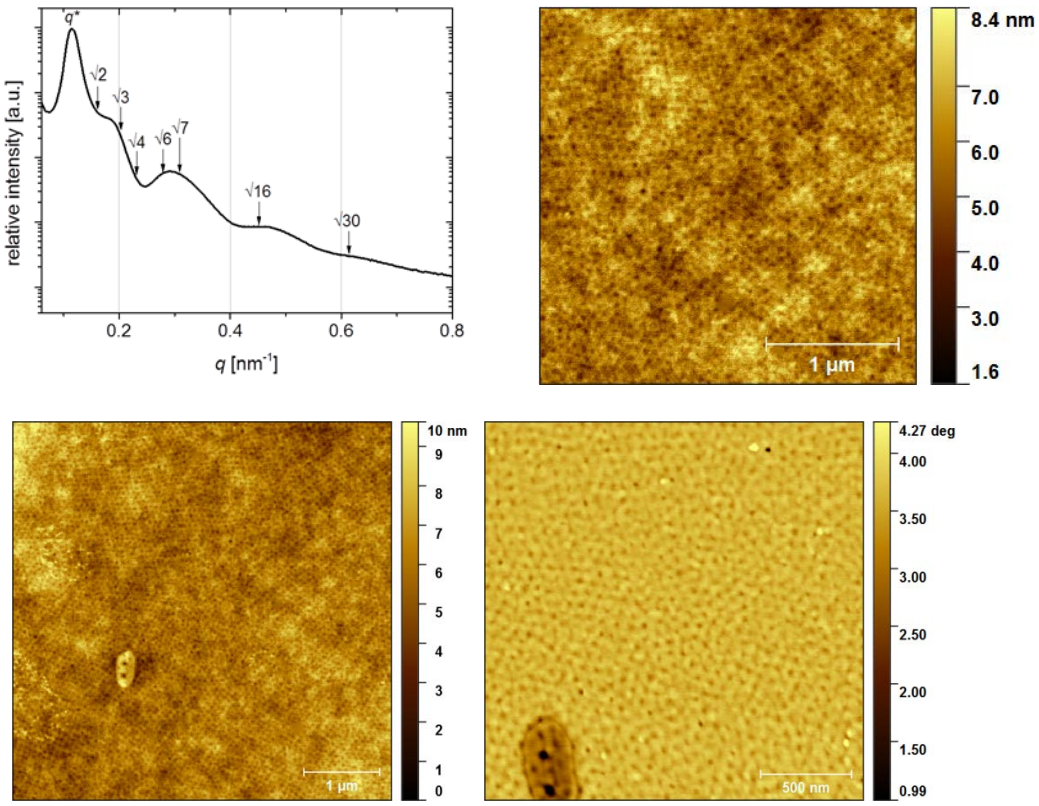

$PS_{94}PMEMA_6^{176}$

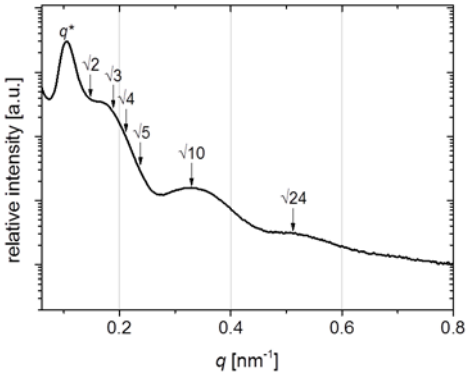

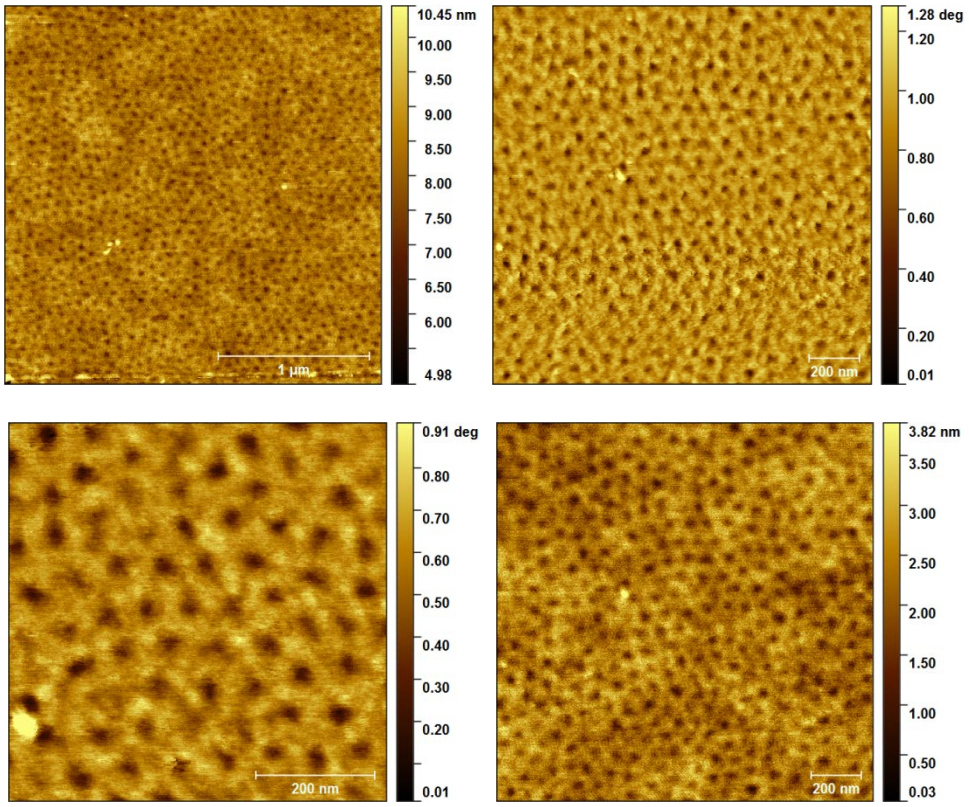

$PS_{82}PMEMA_{18}^{130}$

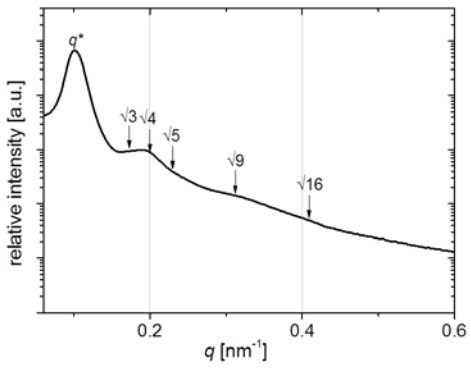

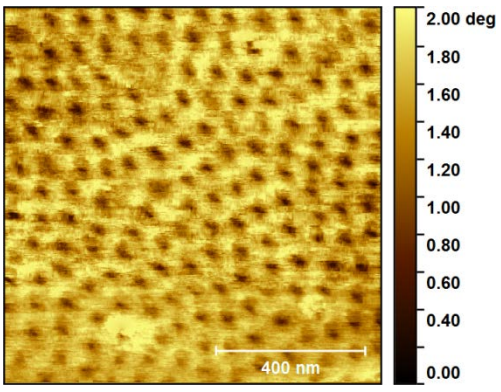

$PS_{70}PMEMA_{30}^{80}$

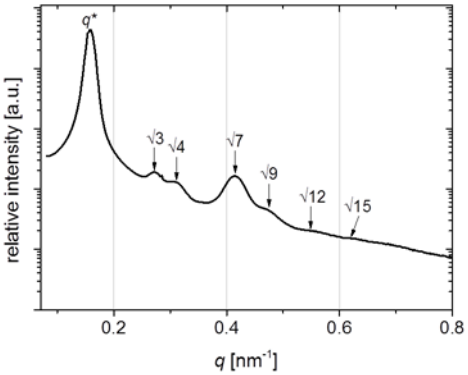

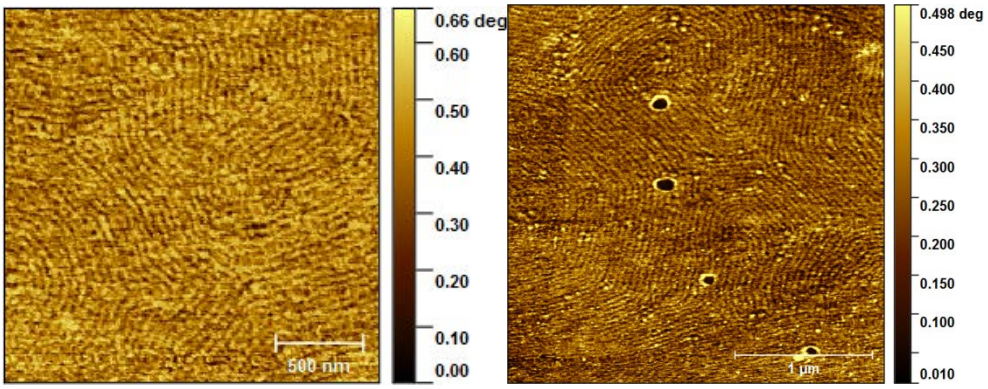

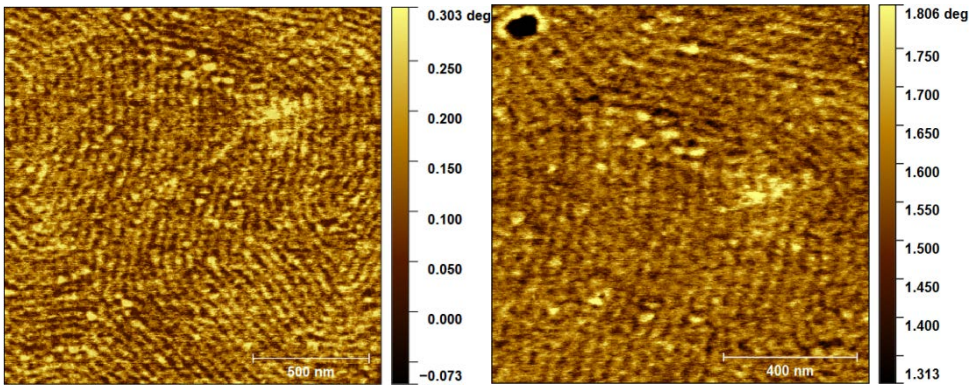

$PS_{77}PMEMA_{23}^{73}$

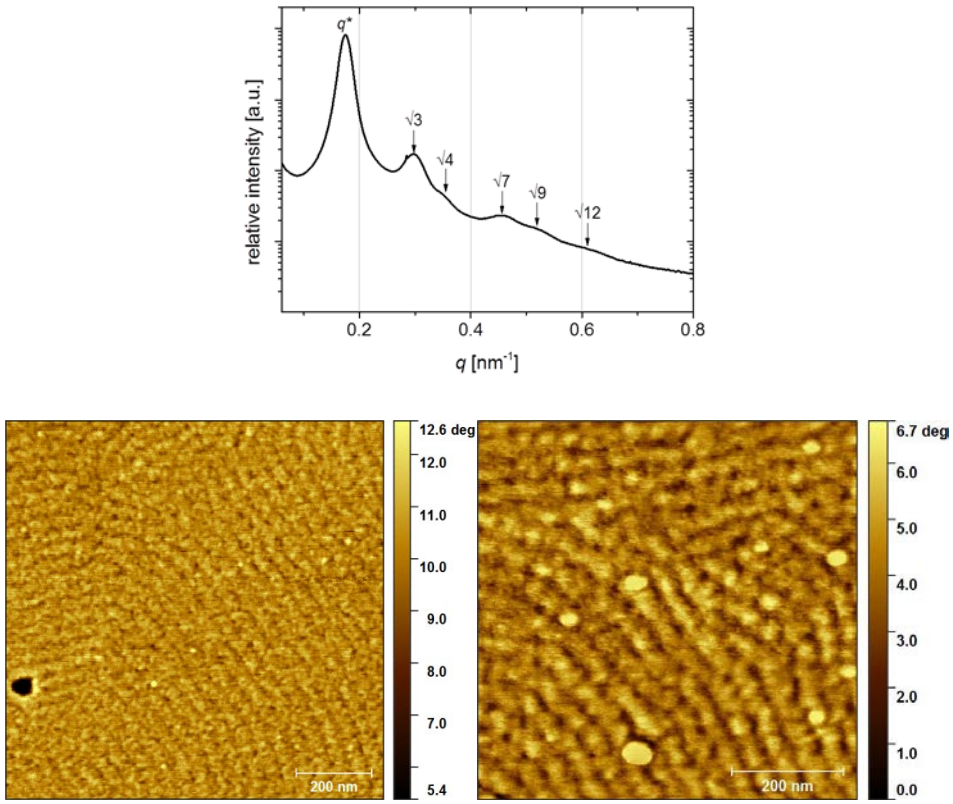

Size Distributions at Different pH

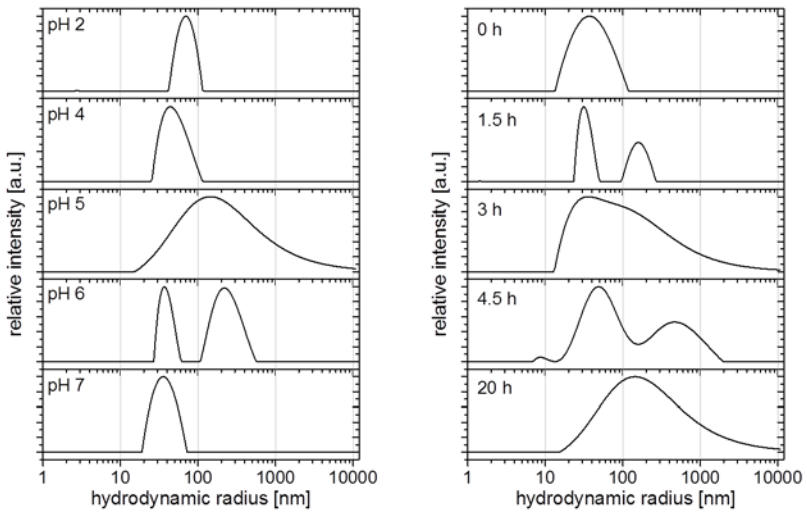

Figure S5 Size distributions (obtained *via* fitting with a CONTIN algorithm) for aqueous micellar solutions of $PS_{67}PMEMA_{33}^{166}$ at different pH-values (left, pH 3 is left out due to high similarity to pH 2) and at different times after HCl addition at pH 5 (right). See Figure 6 for more information.

Solvent Mixtures of 1,4-Dioxane and Water

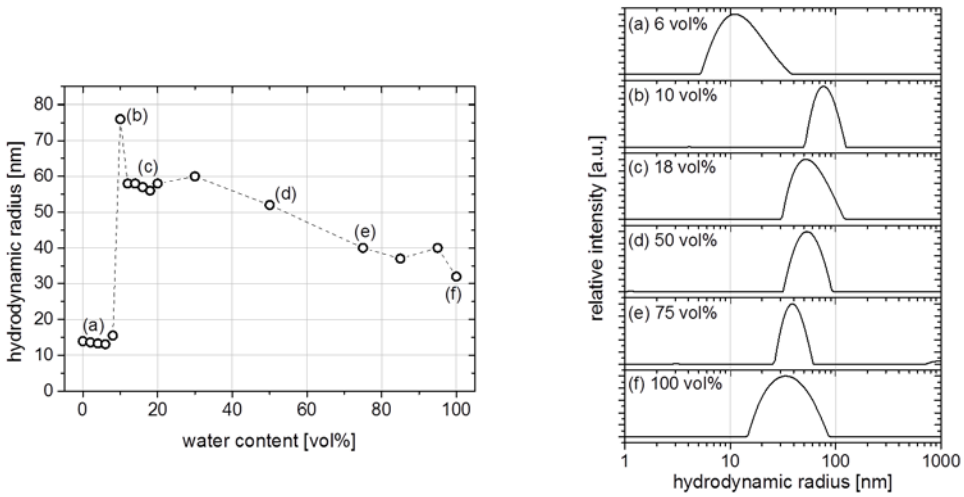

Figure S6 Size distributions (obtained *via* fitting with a CONTIN algorithm) for micellar solutions of $PS_{67}PMEMA_{33}^{166}$ in solvent mixtures of 1,4-dioxane and water (compare to Figure 8). Water contents are indicated in the graphs.

Solvent Mixtures of THF and Water

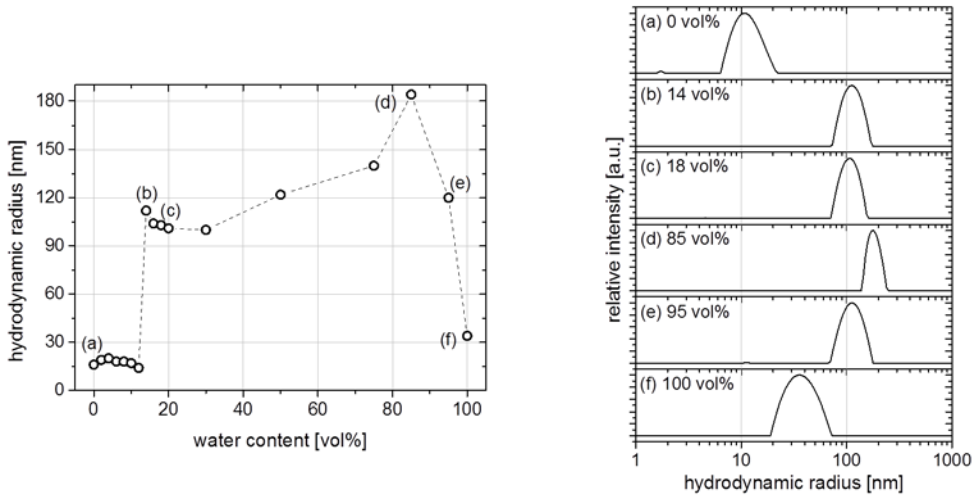

Figure S7 Size distributions (obtained *via* fitting with a CONTIN algorithm) for micellar solutions of $PS_{67}PMEMA_{33}^{166}$ in solvent mixtures of THF and water (compare to Figure 8). Water contents are indicated in the graphs.

PMEMA Homopolymer in 1,4-Dioxane/Water and THF/Water Mixtures

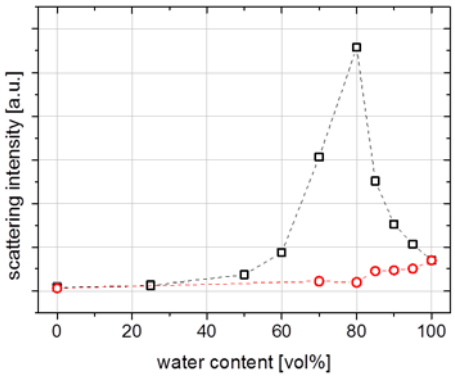

Figure S8 Scattering intensities for solutions of PMEMA homopolymer[a)] ($\overline{M}_n$ = 37 kDa, $Đ$ = 1.12)[b)] in solvent mixtures of THF/water (□) and 1,4-dioxane/water (○), respectively, at room temperature (compare to Figure 8). In THF/water mixtures with medium water contents (40–95 vol%), scattering intensity is increased due to partial aggregate formation.
a) Synthesized as previously reported.[1] b) Determined *via* SEC with eluent THF and PMMA calibration.

References

[1] Eggers S, Fischer B, Abetz V. Macromol Chem Phys 2016;217(6):735-747.